Proceedings of the 16th International Conference on Soil Mechanics and Geotechnical Engineering

doi:10.3233/978-1-61499-656-9-851

Calibration of heterogeneous, probabilistic soil models

Calibrage des modèles hétérogènes et probabilistes de sol

A.L. Rechenmacher, Z. Medina-Cetina & R.G. Ghanem
Department of Civil Engineering, Johns Hopkins University, Baltimore MD, USA

ABSTRACT

This paper demonstrates the applicability of advanced experimental technologies to enhance the state of model–based predictions in soil mechanics. By utilizing imaging techniques to measure local displacements, local non-uniformities in response are captured over a soil sample specimen during a triaxial test. These are assimilated into the solution of an inverse process which yields a description of the spatial variability of the mechanistic parameters of the corresponding constitutive model.

RÉSUMÉ

Cet article démontre l'applicabilité des technologies expérimentales avançées pour augmenter l'état de prévisions modèle-basées dans la mécanique de sol. En utilisant des techniques de formation image pour mesurer des déplacements locaux, des non-uniformités locales dans la réponse sont capturées au-dessus d'un spécimen témoin de sol pendant un essai triaxial. Celles-ci sont assimilées dans la solution d'un processus inverse qui rapporte une description de la variabilité spatiale des paramètres mécanistes du modèle constitutif correspondant.

1 INTRODUCTION

Calibration of soil constitutive models based on triaxial tests traditionally ignores local phenomena such as lateral displacements and localized compressive zones, due to the fact that standard triaxial devices take only global measurements in the loading direction. Therefore, triaxial data is limited to calibrate soil constitutive models, because by utilizing only global measurements an implicit 'homogeneous' soil structure is assumed, and thus the inherent structural heterogeneity of the soil specimen is disregarded.

Recently, digital imaging techniques have been applied successfully to analyze local phenomena in sand specimens, particularly in biaxial tests (Rechenmacher & Finno, 2004) and in triaxial tests (Rechenmacher & Medina-Cetina, 2003; Rechenmacher et al., 2003 and 2004). The authors have used the 3D Digital Image Correlation (3D-DIC) technique to capture 3D full displacement fields by processing sets of digital images taken systematically during a test, yielding tens of thousands of displacement measurements over a continuous specimen surface.

To simulate the test conditions, a 3D finite element model was built to accommodate the actual specimen geometry and effects of boundary conditions. This model was designed to allow the spatial variation of the mechanical parameters of the constitutive model within the sample. Three different level of variability were considered in this work: *homogeneous*, *orthotropic* and *heterogeneous*. To obtain a description of the soil parameter variability within the specimen, an inverse process was solved by minimizing the difference between the displacement fields predicted by the model and those measured in the actual test.

The inverse process was developed using data from different triaxial tests performed under similar conditions as a way to populate a database that will be used to identify the main statistical parameters associated to different soil levels of material variability. Once a comprehensive statistical database is collected and analyzed, it will be possible to apply a probabilistic approach to calibrate soil constitutive models.

2 EXPERIMENTATION

2.1 *Triaxial Tests*

Specimens were prepared using a uniform dry sand and vacuum consolidated to 40 kPa. Tests were conducted in an automated triaxial device that applied the axial load from the bottom of the specimen. Specimens were sheared with a controlled deformation rate of 0.2% of axial strain/min. The sand specific gravity was G_s = 2.63 with a mean diameter D_{50} = 0.5 mm and coefficients of uniformity and curvature, Cu = 2.34 and Cc = 1.11 respectively. A special feature of this sand was the wide color spectrum of its grains, which made it suitable for the pattern recognition needed during the 3D-DIC.

Each specimen was carefully prepared to achieve similar geometric and density characteristics. The specimen's height varied between 154 and 159 mm, with an average diameter of 71.12 mm. Specimens were formed in three layers using a vibratory compaction method, by compacting the surface of each layer uniformly, and by applying a slight vibration on the mold sides. The relative density of all specimens varied between 90 and 95%.

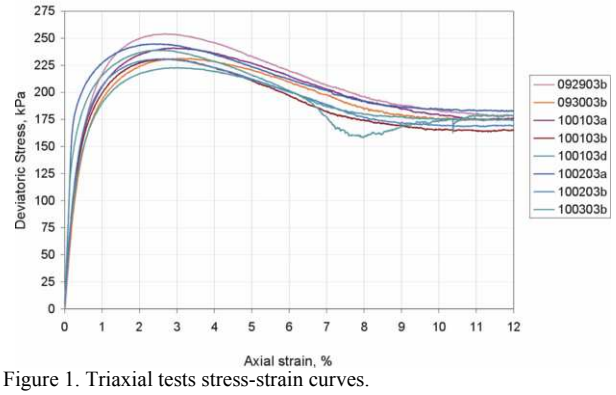

Figure 1. Triaxial tests stress-strain curves.

Figure 1 introduces the stress-strain curves of eight triaxial compression tests that have been analyzed to-date. They represent the global stress-strain behavior of the samples, and were used to estimate the mechanical parameters of the constitutive model considered for the simulation.

2.2 *3D Digital Image Correlation Analysis*

During each triaxial test, pairs digital images were captured simultaneously every 15 seconds (0.05 % of axial strain) using two 14-bit digital cameras Q-Imaging PMI-4201, with 4.2 Mega pixels of resolution. The software used to obtain the 3D displacement fields, VIC-3D, was developed by Correlated Solutions (2004). A key step before the image acquisition is a calibration process, which yields parameters that define a coordinate system that serves as a reference frame where the 3D object shape is traced. Displacement fields are obtained after finding the best match between subsets of uniquely colored pixels on the reference (undeformed) and the target (deformed) images using an appropriate similarity measure, such as the iterative spatial domain cross-correlation algorithm (Sutton et al., 2000). This algorithm introduces a solution method that not only solves for the displacements but also for the rotations and strains and was included in the analysis software. Full-field displacement information is obtained by overlapping pixel subsets. 3D displacement fields could be measured over approximately 90 degrees of the specimen surface.

3 MODELING

A 3D finite element model was built to simulate each one of the triaxial specimens. They included the corresponding sample geometry, which was obtained directly from the reference images. The models also included boundary elements such as the porous stones, located at the bottom and at the top of the specimens, which restrained the soil from any horizontal displacements. The shearing load was applied as a uniformly distributed pressure underneath the bottom porous stone. The confining pressure was applied as a normal stress uniformly distributed all around the specimen surface.

The 3D-DIC analyses revealed a slight displacement at the top of the specimen, which was supposed to be completely motionless. A refined analysis on the boundary between the soil and the top porous stone proved that there was a significant motion due to the equipment compliance. This effect was included in the simulations as a vertical prescribed motion.

An isotropic linear elastic constitutive model was chosen in a first attempt to understand the influence of the materials spatial variability lying within the specimen, into the local phenomena observed over the sample surface. A linear elastic domain common for all tests was chosen between 0.0 % and 0.2 % of axial strain, where the stress-strain ratio or Young's Modulus was observed to be approximately constant. Each model included 1296 eight-node, solid and isoparametric elements, which were integrated implicitly with respect to time. The solver utilized for the simulation was LS-DYNA (Hallquist, 1998).

Three models were built, which considered different levels of material variability or different 'spatially distributed materials' (Figure 2): the *homogeneous* model, with only one 'material' uniformly distributed within the specimen; the *orthotropic* model, with five vertical layers and three horizontal concentric layers, resulting in as many as 15 materials; and the *heterogeneous* model, with five vertical layers, and three concentric layers split vertically in two sections, allowing up to 25 materials.

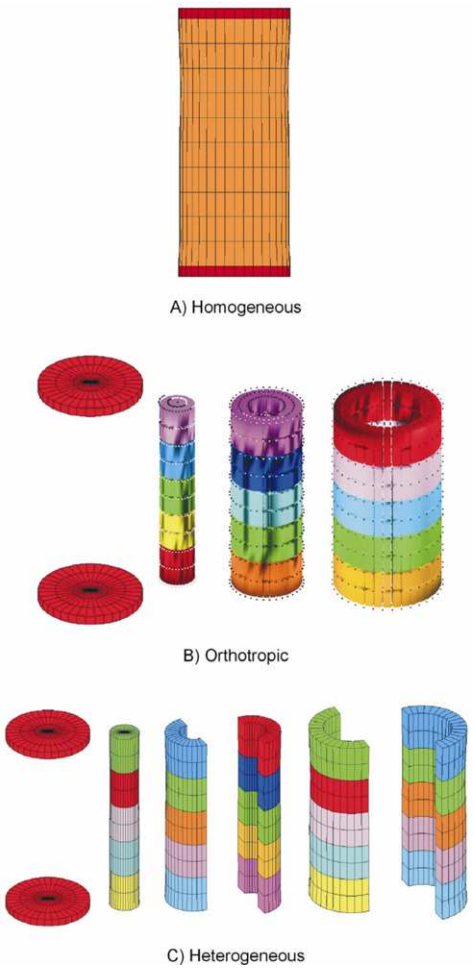

Figure 2. Soil models.

4 INVERSION PROCESS

Measured displacement fields are comprised of three components u(x,y,z,t), v(x,y,z,t) and w(x,y,z,t), corresponding to the x, y and z directions respectively, where x is the frontal horizontal direction, y is the vertical direction along the specimen axis, z is the horizontal direction that goes outward from the specimen, and t is the time at which the images were taken. As a way to incorporate the displacement field information into the inverse process, it was necessary to take local averages of each field over net areas centered at the finite elements nodes located over the model surface (Rechenmacher and Medina-Cetina, 2003). These new fields u_{avg}(x,y,z,t), v_{avg}(x,y,z,t) and w_{avg}(x,y,z,t) were incorporated into an objective function, defined as the weighted sum of the squared difference between the simulated and the measured displacements. The inverse process was solved by allowing the material parameters identified in a particular model to vary independently until the residual of the objective function was minimized. The software used to perform the inverse process was LS-OPT (Stander et al., 2003).

5 PARAMETERIZATION RESULTS

Figure 3 presents the objective functions associated to the *homogeneous*, *orthtropic* and *heterogeneous* models when applied to the data of test 100103b. Two sets of curves are identified in this figure: the first set includes the top two curves, and shows the minimization process when the compliance effect was not included in the modeling (top porous stone is fixed); the

second set consists of the lower three curves, for which the analyses included the compliance effect (top porous stone is moving). Their corresponding initial values for the Young's modulus were 43.226 MPa and 66.803 MPa, which were taken from the global stress-strain curves. A constant value of Poisson's ratio of 0.2 was considered for all cases. The minimum residual values of the first set are higher than those of the second set. This shows the importance of including the equipment compliance effect to capture the actual soil behavior.

The second set of curves, reveal that the gain in terms of the residuals is minimal when the *homogeneous* and the *orthotropic* models are compared to each other. However, when these two are compared with the performance of the *heterogeneous* model, the residual gain is significant, which means that the higher spatial variability in the models, the smaller the difference between the simulated and measured displacements. This means that using a very simple constitutive model it is possible to reproduce structural heterogeneities within the soil specimen that better accommodate the actual test behavior. A similar and consistent behavior was found for the other seven experiments.

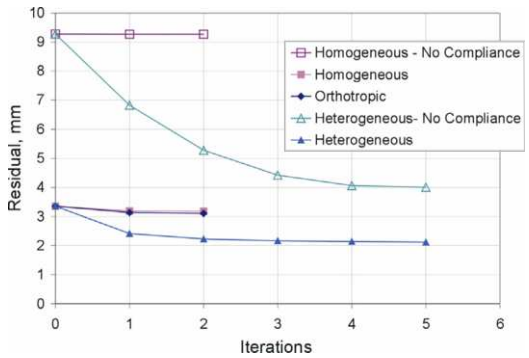

Figure 3. Objective functions.

Figure 4 presents the 'optimized' vertical cross sections of the Young's modulus corresponding to the second set of objective function curves presented in figure 3 (compliance effect included). The *homogeneous* model (left) presents a value of 73.28 MPa distributed uniformly within the specimen. The *orthotropic* model (center) shows stiffer material in the middle-lower region of the specimen with E values varying between 80 and 85 MPa, and softer material in the lower-exterior areas with values varying between 48 MPa and 52 MPa, and in the upper-central region with values close to 59 MPa. The *heterogeneous* model (right), shows a non-symmetric E distribution with higher variability than the orthotropic model but with a similar distribution, having a narrower stiffer region with higher E values close to 109 MPa, and a bigger softer region which extends to the sides of the specimen with E values varying between 25 MPa and 35 MPa in the lower-exterior areas, between 63 and 68 MPa in the upper-central region, and between 50 and 85 on the sides.

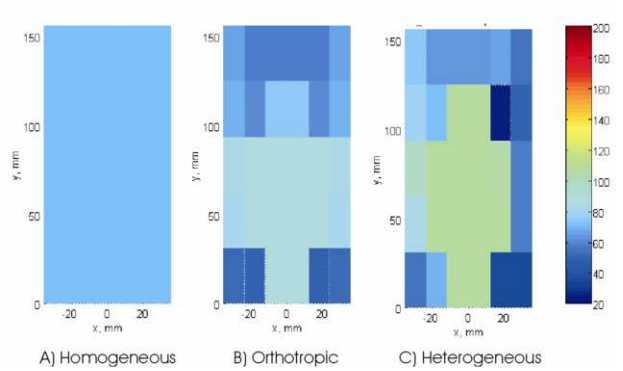

Figure 4. Young's modulus distribution along the specimen's vertical cross section (test 100103b).

A comparison of the heterogeneous model performance in terms of displacements with respect to the actual measurements at 0.2 % of axial strain is introduced in figure 5 (same test 100103b). The heterogeneous parameter variation accommodated fairly well the non-symmetric displacement behavior observed on the u displacement field, and the non-uniform vertical displacements observed on the v displacement field. The *homogeneous* and the *orthotropic* models were limited to a good performance in terms of the v displacement field only. The absolute error distribution between the simulations and the actual measurements for the three displacements fields u, v and w, followed a Gaussian behavior for all parameterizations, but only when the heterogeneous model was utilized.

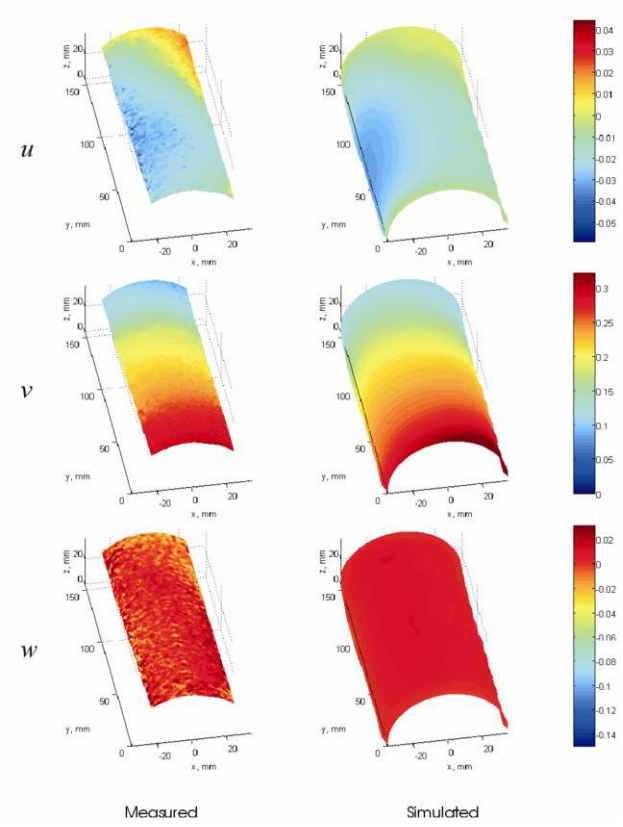

Figure 5. Comparison between simulated and actual displacement fields (test 100103b).

Figure 6 presents the mean and standard deviation of the Young's Moduli corresponding to the eight parameterizations where the heterogeneous model was implemented. Both of them are traced in a normalized x-y space. The mean surface shows a consistent stiffer zone in the middle-lower area and softer regions in the lower-exterior and upper-central areas. The mean values vary between 90 and 115 MPa. On the other hand, the standard deviation surface shows less uncertainty in the middle-lower section (35 MPa) where the stiffer regions are located, whereas the highest uncertainty is found in the lower-exterior and the upper-central areas (55 MPa) where the softer regions are located.

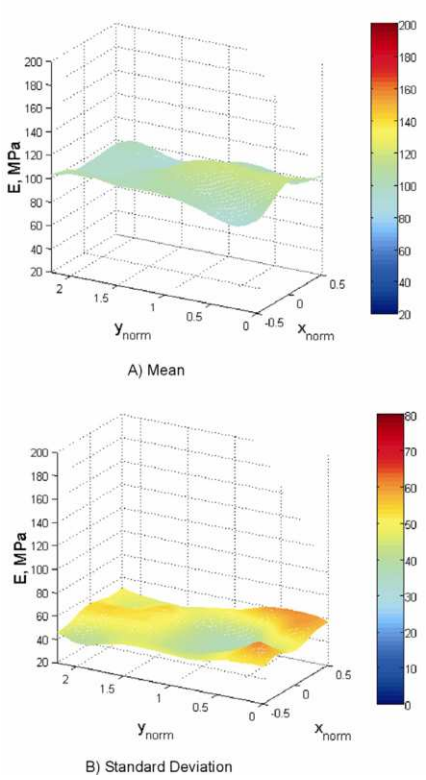

Figure 6. Mean and standard deviation of parameterized tests

Finally, to verify that the parameterization results were consistent with the actual measurements of the Young's modulus (E_{global}), these were compared with their corresponding E optimized distributions ($E_{opt\text{-}avg}$). The correlation coefficient between these two sets of data for the three models was 0.99. Figure 7 presents the correlation between Eglobal and $E_{opt\text{-}avg}$ where the heterogeneous model was implemented.

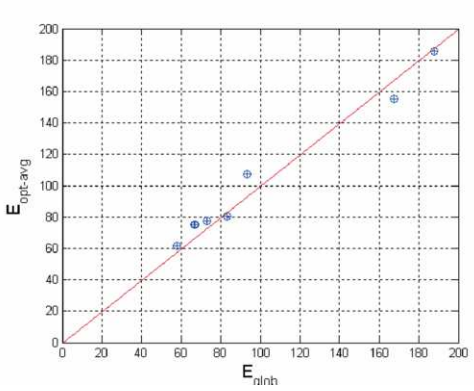

Figure 7. Correlation between E_{glob} and $E_{opt\text{-}avg}$.

6 CONCLUSIONS

It was shown that by combining a predictive model that accounts for the spatial variability of the mechanistic parameters of a linear elastic constitutive model with digital imaging technology that captures local displacement phenomena over the specimen surface during a triaxial test, it is possible to calculate best estimates of the Young's Modulus variability in the interior of the specimen. The analysis of the objective functions corresponding to an illustrative case (test 100103b), showed the importance of considering the compliance effect, which helps to have a more realistic value of the Young's Modulus. It was also observed, that the higher the allowable spatial variability of the 'materials', the smaller the difference between the simulated and the actual measurements over the sample surface. Results where the *heterogeneous* model was implemented showed a non-symmetric and heterogeneous distribution of the Young's modulus E along a vertical cross section of the specimen. Consistent behavior was observed for all tests.

The mean surface of the optimized Young's modulus obtained from all parameterizations revealed a concentration of stiffer material located on the middle-lower section of the specimen, and softer material located in the lower-exterior and upper-central regions within the specimen. The uncertainty associated with the Young's modulus variation was reciprocal to the mean surface, as described by the standard deviation surface, which shows higher uncertainty regions where the softer soils were found, and lower uncertainty regions where the highest stiffness values were found. A comparison of the average values of each of the optimized Young's modulus distributions ($E_{opt\text{-}avg}$) corresponding to the eight parameterizations, with their corresponding global measurements (E_{global}), taken from the global stress-strain curves, showed that the inversion process yielded consistent results.

REFERENCES

Correlated Solutions. 2004. http://www.correlatedsolutions.com

Hallquist J.O. 1998. LS-DYNA: Theoretical Manual, Livermore Software Technology Corporation. Livermore, CA, USA.

Rechenmacher A.L. and Finno, R.J. 2004. Digital Image Correlation to Evaluate Shear Banding in Dilative Sands. *Geotechnical Testing Journal*, 27, No. 1. 1-10.

Rechenmacher A.L. and Medina-Cetina Z. 2003. Digital Imaging-Based Measurements of Deformed Shapes of Axisymmetric Soil Specimens. Proceedings 16th ASCE Engineering Mechanics Conference, Seattle, WA, July 16-18.

Rechenmacher A.L., Medina-Cetina Z. and Ghanem R.G. 2003. Predictions for Heterogeneous Soil Behavior: Assimilation of Digital Imagery into Finite Element Models of Sand. LSD2003: International Workshop on Limit State Design in Geotechnical Engineering Practice, Cambridge, MA, June 26.

Rechenmacher A.L., Medina-Cetina Z. and Ghanem R.G. 2004. Calibration of Soil Constitutive Models with Heterogeneous Parameters. 9th ASCE Specialty Conference on Probabilistic Mechanics and Structural Reliability, Albuquerque, NM, July 26-28.

Stancer, N., Eggleston T., Craig K. and Roux W. 2003. LS-OPT User's Manual: Design Optimization Software for the Engineer Analyst. Livermore Software Technology Corporation. Livermore, CA, USA.

Sutton, M.A., McNeill, S.R., Helm, J.D. and Chao, Y.J. 2000. Advances in Two-Dimensional and Three-Dimensional Computer Vision. Photomechanics. *Topics in Applied Physics*, 77, 323-372.